



## Three-dimensional texture analysis of aligned carbon nanotube structures



Seyram Gbordzoe<sup>a</sup>, Sergey Yarmolenko<sup>b, \*\*</sup>, Yu-Yun Hsieh<sup>a</sup>, Paa Kwasi Adusei<sup>a</sup>,  
Noe T. Alvarez<sup>c</sup>, Svitlana Fialkova<sup>b</sup>, Vesselin Shanov<sup>a, c, \*</sup>

<sup>a</sup> Department of Mechanical and Materials Engineering, University of Cincinnati, Cincinnati, OH 45221, United States

<sup>b</sup> Department of Mechanical Engineering, Engineering Research Center, North Carolina A&T State University, Greensboro, NC 27411, United States

<sup>c</sup> Department of Biomedical, Chemical and Environmental Engineering, University of Cincinnati, Cincinnati, OH 45221, United States

### ARTICLE INFO

#### Article history:

Received 3 April 2017

Received in revised form

7 June 2017

Accepted 9 June 2017

Available online 12 June 2017

### ABSTRACT

The alignment of different carbon nanotube (CNT) structures has been studied extensively using varying techniques. Most of these techniques however do not present a true three-dimensional (3D) representation of the orientation of the material. In this work, the orientation distribution functions obtained from X-ray pole figures for different CNT structures (vertically aligned CNT arrays, randomly orientated buckypaper and horizontally aligned CNT sheets) are presented. This technique is also used to examine the effects of solvent densification and stretching on the alignment of CNT sheets. It has been demonstrated that depending on the solvent used for densification, the alignment achieved varies as the elongation is increased. The physical properties of CNT sheets are shown to depend on the alignment and solvent used for densification. The most aligned CNT sheets densified with acetone and ethanol reveal an increase in tensile strength of 140% and 58% respectively over unaligned sheets.

© 2017 Elsevier Ltd. All rights reserved.

### 1. Introduction

Carbon nanotubes (CNTs), simply described as a graphene sheet rolled into a tube, have been shown to have excellent mechanical, electrical and thermal properties [1–3]. Exploiting these materials on the macroscale requires better processing methods such as improved alignment and densification. The densification of CNTs has been shown to depend on the type of solvent used with better densified CNTs showing better mechanical and electrical properties [4,5]. The alignment of CNT structures, which include arrays, sheets, buckypaper and composites, is important because it affects the physical properties of such materials [6–13]. Spinnable CNT arrays are used for producing horizontally aligned CNT sheets through dry-drawing from an array [14–18], which can be further aligned by different post-processing methods. Stretching is a popular post-processing method that is especially useful for alignment of CNT sheets. It has been reported that an increase in the stretch ratio

leads to a decrease in wavy CNTs in CNT sheets and CNT-polymer composites, which causes more nanotubes to effectively take part in the load bearing process [19–21]. There is however a need to regulate how much strain the nanotubes are placed under since an excess of strain leads to the nanotubes splitting and breaking. This causes a decline in physical properties such as mechanical strength [19,22]. Post-pressing has also been used as a method to both align CNT sheets and improve their density leading to an improvement in physical properties [9,23]. A synergistic approach combining pressing and stretching can also be employed as demonstrated by Liu et al. [22]. Other techniques such as microcombing have been explored to improve the alignment of CNT sheets thereby increasing its physical properties, as demonstrated by Zhang et al. [24,25].

Scattering methods, such as polarized Raman spectroscopy, small-angle X-ray scattering (SAXS), and wide-angle X-ray scattering (WAXS) are useful for analyzing the alignment of CNT structures. Polarized Raman has been used extensively to study alignment of different CNT assemblages [22,23,26–31]. In this paper we will be concentrating more on X-ray scattering methods. Wang et al. were able to investigate the alignment of CNT films by observing relative SAXS intensities as a function of the azimuthal angle [32]. Bedewy et al. and Meshot et al. showed how X-ray

\* Corresponding author. Department of Mechanical and Materials Engineering, University of Cincinnati, Cincinnati, OH 45221, United States.

\*\* Corresponding author.

E-mail addresses: [sergey@ncat.edu](mailto:sergey@ncat.edu) (S. Yarmolenko), [vesselin.shanov@uc.edu](mailto:vesselin.shanov@uc.edu) (V. Shanov).

scattering could be used in determining the alignment of CNT forest during growth [33,34]. They employed the Herman's orientation function (HOF) to calculate the level of alignment of the forest. Mahanandia et al. also used SAXS to verify the parallel nature of CNTs grown at different temperatures [35]. The alignment of CNTs in a CNT/epoxy composite oriented by the magnetic assisted method was examined by Moaseri et al. [36]. They also correlated the alignment of CNTs to the mechanical properties of the composites showing that randomly oriented tubes in the tested samples had a lower strength than those with aligned CNTs.

Most of these techniques are however based on one dimensional (1D) [26,27,37,38] and two-dimensional (2D) [32,33,39–42] reconstruction of the orientation distribution function (ODF). Values of HOF in 1D and 2D orientation analysis depend on alignment between preferred orientation in sample and analytical axis (1D) or plane (2D) [43]. To avoid this limitation, a complete three-dimensional (3D) construction of the ODF for orientated fibrous materials is needed. Generally this can be achieved with pole figure texture analysis [44] which allows the evaluation of ODF intensities in relation to the specimen geometry. The advantages of this technique include: (i) independence from sample alignment, (ii) providing texture analysis of the sample that is averaged over a large area, (iii) producing more accurate and repeatable results which would make it possible to monitor small changes in alignment (such as the effect of stretching or chemical treatments) and (iv) allowing the analysis of polymodal aligned materials (multi-layered, woven, twisted, twinned, etc.) through the wealth of texture analysis methods available. Pole figure analysis has been practiced extensively in studying the texture of polymer fibers [45–48] but its use has been limited in studying the alignment of CNT structures due to very low intensity of its X-ray diffraction. The X-ray diffraction pattern of CNTs is similar to the pattern of graphite. Highly oriented pyrolytic graphite (HOPG) has a sharp characteristic peak at  $26.47^\circ$  with a half-width of  $0.105^\circ$  which corresponds to an interlayer spacing of  $3.36 \text{ \AA}$  of the (002) plane. Intensity of (002) peaks for CNTs strongly depends on nanotube orientation against an incident X-ray beam and therefore orientation distribution of (002) peak intensities can be used for evaluation of alignment of CNTs.

In this study, we introduced pole figures and their corresponding ODF models as a tool in studying the orientation of different CNT structures. We also used this technique to analyze the effects of processing methods such as stretching and solvent densification on the alignment of CNTs in sheet assemblies. Finally, the physical properties namely mechanical and electrical are correlated with the alignment results of the CNT sheets.

## 2. Experimental methods and techniques

### 2.1. MWCNT samples

Spinnable vertically aligned CNT arrays were grown with an ET3000 chemical vapor deposition (CVD) reactor from CVD Equipment Corporation and the experimental procedure is described elsewhere [49]. CNTs grown by this method are predominantly multi-walled with about 1 - 6 walls, average diameter of 10 nm and length of 400 - 450  $\mu\text{m}$ . Transmission electron microscopy (TEM) images of CNTs are presented in Fig. S1 in the supplementary information. These arrays were used for making 100 layer horizontally aligned MWCNT (HA-MWCNT) sheets with the dry-drawing process in a similar way to that published earlier by our group [18]. Pristine CNT sheets have been investigated here as well as densified and stretched sheets.

Buckypaper samples made by the vacuum filtration technique were also studied. General Nano LLC supplied buckypaper samples.

### 2.2. Stretching of CNT sheets

MWCNT sheets were densified with two different organic solvents (acetone and ethanol) and stretched to study the effect of solvent densification and stretching on alignment. A schematic of the process is shown in Fig. 1a and an image of the actual set-up is displayed in Fig. 1b. After MWCNT sheets were fabricated by the drawing method, they were transferred onto a template before being clamped in the stretching apparatus. The samples were then stretched in the presence of the solvent to the pre-determined elongation and left to dry in air for an hour. The amount of solvent added to each MWCNT sheet was 5 ml delivered with a pipette. A digital micrometer (resolution =  $1 \mu\text{m}$ ) was used to accurately measure the pre-determined elongation. The samples were stretched to 0.5%, 1% and 1.5% of the initial length (which was 50 mm for all specimens). One and the same array was used to make CNT sheets for each solvent treatment stretched to the different stretch ratios.

### 2.3. X-ray diffraction

A Bruker AXS D8 Discover diffractometer with a  $\text{Cu K}\alpha$  X-ray radiation, parallel beam optics, 1D LynxEye PSD detector and centric Eulerian cradle was used for X-ray diffraction (XRD) experiments. The MWCNT samples were aligned parallel to X-ray beam using XY tilt stage with sample stretching capability. Pole figure measurements were performed at full rotation ( $\psi$ ) and  $0-80^\circ$  tilt ( $\chi$ ) of sample with a step of  $5^\circ$  at a rate of 10 s per step. Intensities of aligned CNTs were recorded at  $2\theta = 26^\circ$  (002 graphitic peak), while background correction was done by linear approximation of X-ray scattering intensities at  $20^\circ$  and  $31.6^\circ$ . Processing of pole figure data was done with the MTEX version 4.2.1 toolbox for Matlab. A description of this toolbox and the Matlab script used for processing pole figure data is provided in the supplementary information.

### 2.4. Characterization methods

Surface morphologies of the different MWCNT structures were studied using an FEI XL30 scanning electron microscope (SEM).

The tensile strength of the MWCNT sheet samples was measured using a uniaxial tensile testing machine (Instron 5948). A laser micromachining system by Oxford Lasers was employed to cut CNT sheets for tensile tests. The samples were tested in the longitudinal direction (parallel to the drawing direction) and had a gauge length of 22 mm, width of 1 mm and strain rate of 1 mm/s for all experiments. The average thickness of the acetone and ethanol densified sheets was measured with SEM to be  $4.95 \mu\text{m}$  and  $5.46 \mu\text{m}$  respectively as presented in Fig. S2 in the supplementary information. The samples were tested at ambient temperature and pressure.

Measuring the sheet resistance for the samples and multiplying it by the sheet thickness calculated the electrical conductivity for the samples. Sheet resistance was measured in the longitudinal direction using a Jandel 4-probe instrument (Model RM3000).

## 3. Results and discussion

### 3.1. Pole figure analysis of MWCNT structures

Non-aligned MWCNTs have shown very weak X-ray diffraction from concentric graphitic shells. Alignment between MWCNTs increases the intensity of graphitic peaks. This phenomenon has been used for rough estimates of alignment in MWCNT-polymer matrix composites [24]. However, very low intensity of graphitic X-ray diffraction in composites and CNT arrays does not allow performing detailed investigation of alignment. Therefore, latest studies of

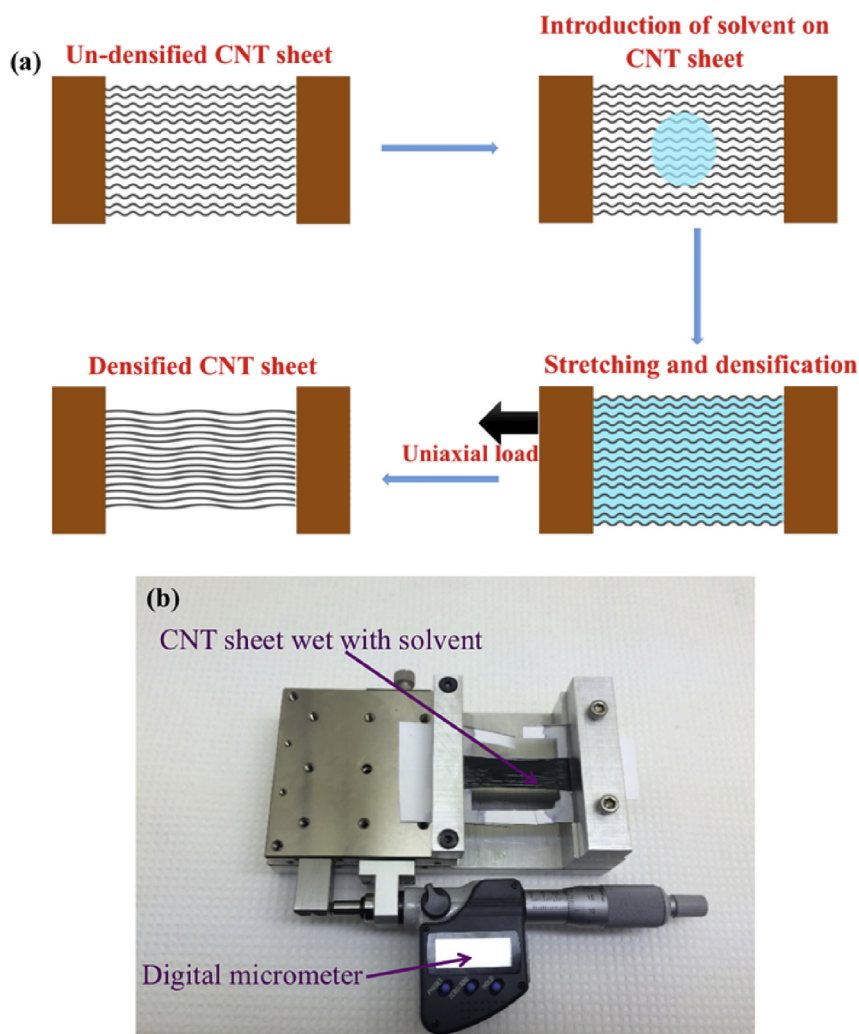


**Fig. 1.** (a) Schematic illustration of wet stretching of CNT sheets with solvents; (b) picture of wet CNT sheet clamped in stretching set-up. (A colour version of this figure can be viewed online.)

alignment in MWCNT-based materials were conducted by utilizing synchrotron SAXS method [33] based on analysis of azimuthal distribution of scattering from diameters of CNTs at angles below  $1^\circ$ . HA-MWCNT sheets have relatively high intensity of graphitic diffraction allowing acquisition times in the range of 10–20 s per point using 1D or 2D detectors on laboratory XRD equipment. Therefore, we evaluated the capability of laboratory qualitative analysis of alignment in MWCNT-based materials using 3D texture analysis. This was performed by moving the samples in two angles ( $\psi$  and  $\chi$ ).  $\psi$  is the rotation angle and can be alternated from  $0^\circ$  to  $360^\circ$  while  $\chi$  is the tilt angle and can travel from  $0^\circ$  to  $90^\circ$ . For a fully oriented MWCNT material aligned in the  $xy$  diffraction plane where  $x$  is the X-ray direction at  $\Theta = 0^\circ$ , the intensity of (002) peak due to diffraction from equally distanced tubular graphitic sheets does not depend on rotation around  $z$ -axis ( $\chi = 0^\circ$ ,  $\psi$ -scan) as shown in Fig. 2a. Due to the tubular structure of nanotubes, the intensity of the (002) peak also does not depend on rotation around  $x$ -axis if the MWCNT's axis is aligned with  $x$ -axis ( $\psi = 0^\circ$ ,  $\chi$ -scan) as shown in Fig. 2b. In Fig. 2c, diffraction from fully oriented MWCNTs should be negligibly small. In the case of a partially orientated material, intensity of (002) peak should be highest at geometries shown in Fig. 2a and b while at other geometries shown in Fig. 2c, the intensity is suppressed depending on MWCNT alignment in

material and tilt angle  $\chi$ .

This analysis supports typical changes of intensity of graphitic peak in MWCNT-based materials measured at different sample directions (Fig. 3). Diffraction patterns of HA-MWCNT sheets presented by dotted, black and red lines in Fig. 3a correspond to geometries presented in Fig. 2a–c respectively. A graphitic peak (002) of HA-MWCNTs aligned along direction of X-ray beam ( $\psi = 0^\circ$ ,  $\chi = 0^\circ$ ) was observed at  $26.03^\circ$ , which corresponds to a 3.42 Å spacing between concentric graphitic shells within the tubes (dotted line in Fig. 3a). The peak has decent intensity compared to background level, wide (FWHM =  $2.11^\circ$ ) and asymmetric with center mass at  $25.68^\circ$ . The low angle shoulder in the peak indicates the presence of inter-tube contacts between aligned MWCNTs [50]. Diffraction pattern of vertically aligned ( $\psi = 90^\circ$ ,  $\chi = 0^\circ$ ) and schematically shown in Fig. 2a and horizontally aligned ( $\psi = 0^\circ$ ,  $\chi = 0^\circ$ ), schematically shown in Fig. 2b, and shown by dotted line in Fig. 3a for HA-MWCNT sheets are identical. Although rotation around  $x$ -axis in horizontally aligned sample ( $\psi = 0^\circ$  and  $\chi = 0^\circ$ , dotted line) should not have an effect on diffraction, peak intensity of tilted sample slowly decreases with increase of tilt angle  $\chi$  due to lowering effective volume of interacting MWCNTs in flat film-like tilted samples. An example of this intensity decrease is presented by the pattern of tilted horizontally aligned sample ( $\psi = 0^\circ$  and

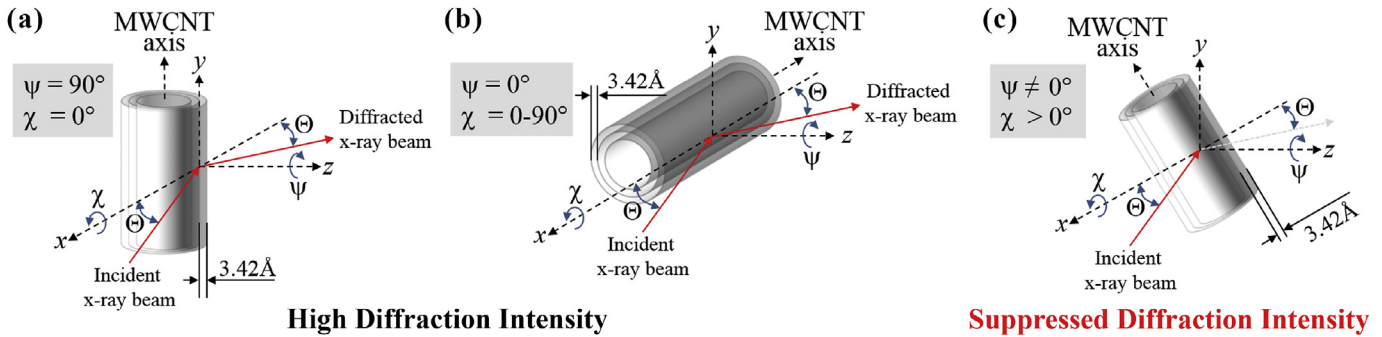


Fig. 2. Analysis of diffraction intensity at different  $\psi$  and  $\chi$  rotations. (A colour version of this figure can be viewed online.)

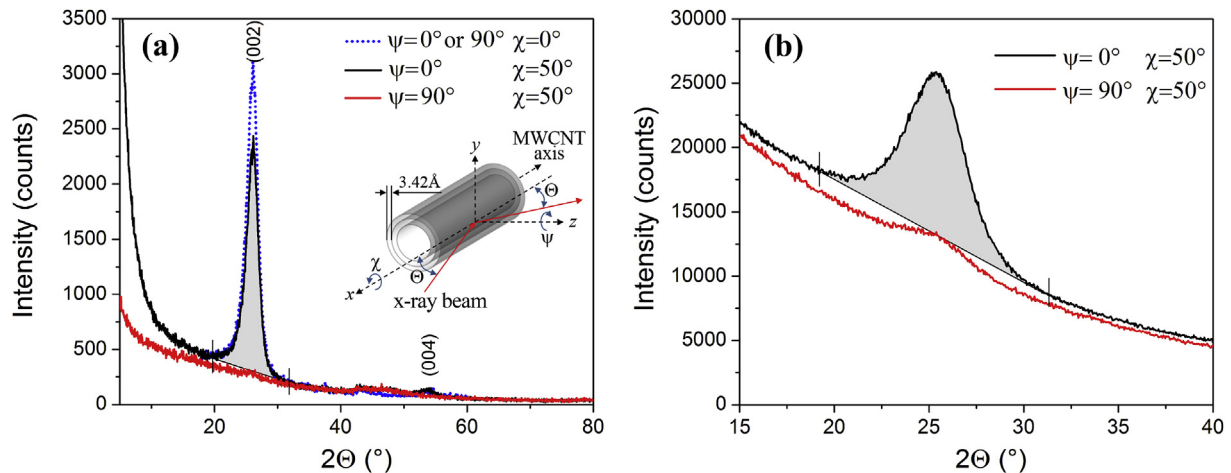


Fig. 3. XRD pattern of MWCNT at different  $\psi$  and  $\chi$  rotations for (a) HA-MWCNT sheet and (b) 10 mm tall MWCNT array. (A colour version of this figure can be viewed online.)

$\chi = 50^\circ$ , black line in Fig. 3a). This phenomenon is known as X-ray beam defocusing effect and can be corrected in pole figures. Tilting of vertically aligned sample ( $\psi = 90^\circ$ ,  $\chi = 0^\circ$ , dotted line) sharply reduces intensity of (002) peak, and at  $\chi = 50^\circ$  this peak disappears (red line) suggesting that the sample has good alignment of nanotubes along preferred orientation and it does not have detectable amount of nanotubes with misalignment  $\geq 50^\circ$ .

Fig. 3b shows corresponding diffraction patterns for a 10 mm tall MWCNT array similar to that previously grown by our group [51]. This array is different from that used to produce CNT sheets studied in this work. A taller MWCNT array sample was used in order to get an improved diffraction intensity. The sample however still has very weak, almost two times less intensity than background level, very wide (FWHM =  $3.45^\circ$ ) and asymmetric graphitic peak at  $25.48^\circ$  ( $d = 3.49 \text{ \AA}$ ) with center mass at  $25.06^\circ$ . In contrast to HA-MWCNT sheets shown in Fig. 3a, at any sample geometry of MWCNT array we detected contribution of (002) peak (red). All these observations indicate significantly lower degree of alignment in the 10 mm tall MWCNT array compared to MWCNT sheets.

Based on the analysis above we considered that the alignment of MWCNTs could be characterized by the fiber properties of the ODF. The pole density of a pole figure is related to the ODF by the following expression:

$$P_{(hkl)} = \frac{1}{2\pi} \int_0^{2\pi} f(\psi, X, Y) dY \quad (1)$$

where  $P_{(hkl)}$  is the pole density at a particular crystallographic plane

( $hkl$ ),  $f(\psi, \chi, \gamma)$  is the 3D ODF with  $\gamma$  being the angle at which the pole figure defined by the angles  $\psi$  and  $\chi$  can be rotated to represent the third dimension. Therefore knowing the pole figure data of a sample, the ODF can be derived through a process known as pole inversion. Since the (002) diffraction peak of MWCNT-based materials is located in the range of significant background scattering, in order to receive the correct pole figure data it is important to use the integral intensity of the peak without background (shown as grayed area under peak in Fig. 3a and b). Background component should be calculated for every geometry because it significantly depends on orientation and it is influenced by the distribution of inter-tube contacts between MWCNTs [50]. We assume a linear background profile between  $2\theta$  of  $20^\circ$  and  $31.6^\circ$ . Therefore to get the corrected pole figure data, the average intensity at  $2\theta$  of  $20^\circ$  and  $31.6^\circ$  was subtracted from the intensity at the main peak at  $2\theta = 25.8^\circ$  for every measured tilt  $\psi$  ( $0-80$ ) and azimuthal  $\chi$  ( $0-360$ ) angles. MTEX toolbox was used for calculating the pole figures and the corresponding ODF models.

The orientation of three different MWCNT structures was studied using the pole figure analysis method and the obtained ODF models and profiles are shown in Fig. 4. The ODF model results show a spread of orientation of the MWCNT fibers along the axis of interest with an intensity color scale bar on the right. The ODF profile also shows a distribution of orientation of the material being analyzed. MWCNT array and pristine HA-MWCNT sheet which were mounted with the alignment direction parallel to the X-axis have the main peaks located at  $180^\circ$  and  $360^\circ$  for the azimuthal scan. For the MWCNT array results presented in Fig. 4a, b it can be seen that there is a big spread in the orientation distribution along

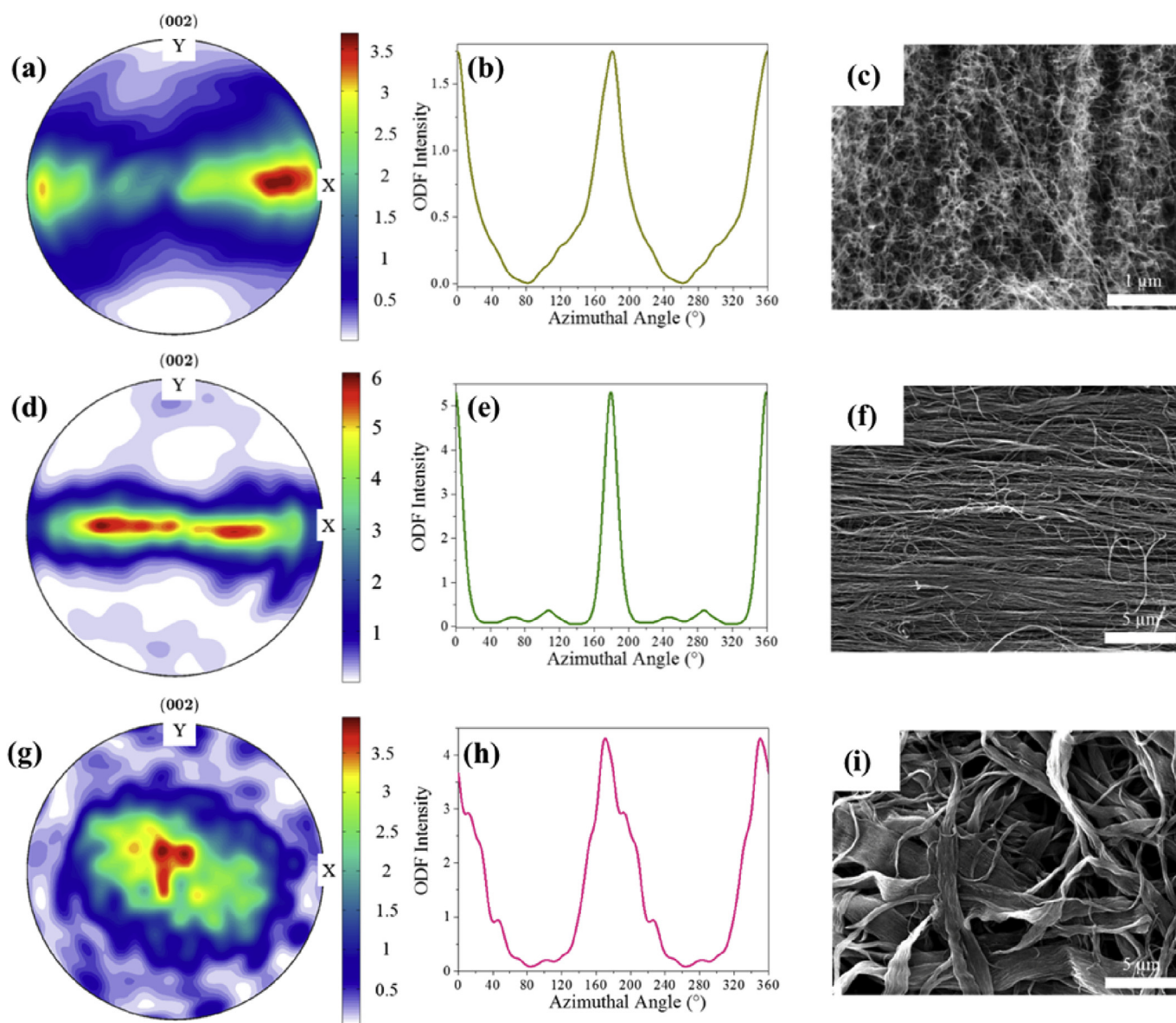


**Fig. 4.** From left to right, ODF model, ODF profile and SEM image of (a, b, c) 10 mm tall MWCNT array, (d, e, f) pristine HA-MWCNT sheet and (g, h, i) buckypaper. (A colour version of this figure can be viewed online.)

the azimuthal axis because nanotubes are wavy and not really aligned as can be seen in the SEM image (Fig. 4c). The image shows MWCNT bundles with a very wavy nature, which explains the lack of alignment seen in the ODF model and profile. Pristine HA-MWCNT sheet on the other hand has significantly higher alignment than MWCNT array and buckypaper. It can be seen that the ODF model and profile have significantly higher intensity and narrower spread in distribution. Better alignment of pristine HA-MWCNT sheet is supported by the SEM image in Fig. 4f. In contrast, the buckypaper sample that has a random orientation does not show any main peaks (Fig. 4g–i). Next we discuss how this technique can be used to show small differences in alignment of densified and stretched HA-MWCNT sheets.

### 3.2. Orientation studies of stretched HA-MWCNT sheets

HA-MWCNT sheets were stretched and densified with acetone

and ethanol at different elongations. These solvents were chosen because they have been used extensively in literature to densify CNT sheets [4,9,11,25,52]. Video S1 in the supplementary information shows a time-lapse movie for an acetone-densified sheet being stretched and densified. It can be seen that the sample undergoes four main post-processing stages: introduction of the solvent, stretching, densification and finally drying. The used solvents have been shown to have different wetting properties. Wetting of CNTs by solvents usually relies on two factors: surface tension and viscosity [53,54]. The surface tension for acetone and ethanol are 23.32 dyn/cm and 22.32 dyn/cm respectively. While their viscosity is 0.31 cP and 1.07 cP for acetone and ethanol respectively. It has been shown that the lower the viscosity, the faster the infiltration time [54]. The infiltration time is described as the time needed for the defined volume of solvent to initially soak into the CNT sheet. The average infiltration times for acetone and ethanol solvents were 104s and 280s respectively. After infiltration, CNT sheets were left to dry in air for 1 h in the stretching set-up before being taken

off. Drying in a fume hood for 24 h to completely remove the solvent followed this step. Another factor that can be taken into consideration is the boiling point of the solvents with acetone and ethanol having boiling points of 56 °C and 78 °C respectively. The boiling point affects the evaporation rate and is therefore expected to play a role in the densification and alignment of the sheets.

Supplementary video related to this article can be found at <http://dx.doi.org/10.1016/j.carbon.2017.06.028>.

For acetone-densified and stretched sheets, the ODF model and profile show a small spread along the azimuthal direction (X-axis) indicating that the MWCNT sheets have a high degree of nanotube axial orientation along the sheet drawing direction as seen in Fig. 5. The ODF profile becomes narrower with increasing stretch ratio, which indicates that the alignment increases with increasing stretch ratio. SEM images show fewer bigger bundles formation due to fast drying and infiltration of the acetone-densified CNT sheets. However for ethanol-densified sheets, a different outcome can be seen. The un-stretched ethanol-densified sheet shown in Fig. 6a displays relatively low alignment indicated by the wider distribution in the ODF model. Alignment was slightly improved by stretching to 0.5%. This was accompanied by the formation of bigger bundles for ethanol-densified sheets compared to acetone-densified sheets, which is clearly seen by the SEM image and inset in Fig. 6f. Stretching to 1% resulted in improvement in alignment while increase of stretching to 1.5% led to decrease of intensity compared to corresponding data for acetone-densified sheets.

The differences in alignment for acetone and ethanol densified sheets are due to different wetting capabilities of the solvents. Ethanol has a higher viscosity and boiling point and therefore it takes a longer time for the solvent to completely wet and evaporate from the CNT sheets. This longer time allows the CNT fibers to form bigger bundles during drying and stretching. In contrast to ethanol, acetone has lower viscosity and boiling point. Therefore, due to fast drying and infiltration of the acetone-densified CNT sheets, there were fewer bigger bundles observed (Fig. 5c, f, i and l).

### 3.3. Alignment analysis of stretched and densified sheets

The quantitative analysis of the alignment of stretched and densified sheets was done by fitting the ODF profiles from the data obtained in the previous section and calculating the Herman's orientation function (HOF).

The HOF is often used to describe the degree of orientation and it is given by the equation:

$$\text{HOF} = \frac{3 \langle \cos^2 \phi \rangle - 1}{2} \quad (2)$$

$$\text{where } \langle \cos^2 \phi \rangle = \frac{\int_0^{\frac{\pi}{2}} I(\phi) \cos^2 \phi \sin \phi d\phi}{\int_0^{\frac{\pi}{2}} I(\phi) \sin \phi d\phi} \quad (3)$$

$I(\phi)$  is the intensity of non-isotropic part of ODF at misalignment angle  $\phi$  against preferred orientation at maximum of ODF [32], and  $\langle \cos^2 \phi \rangle$  is known as the orientation parameter. The HOF has a value of unity when the normal of the reflection plane is parallel to the reference axis and a value of 0 for a randomly orientated sample. For systems with low orientation, evaluation of HOF significantly depends on the method of separation of non-isotropic and isotropic parts of the ODF [26]. The shape of ODF plays a significant role for studies related to the mechanism of CNT growth [33,39,40]. This also applied to processing of composite materials [55] and in all

cases detailed analysis requires an appropriate model for fitting of ODF [39]. Two different fitting functions; Gaussian and Lorentzian were used to fit the ODF profile and calculate the HOF. The HOF results are presented in Table 1 as HOF-L and HOF-G for Lorentzian and Gaussian fits respectively. As can be seen in Table 1, depending on the fitting function used, the HOF values for both acetone and ethanol densified sheets varied. The Lorentzian function has HOF values ranging from 0.564 to 0.580, but the Gaussian function has HOF values ranging from 0.939 to 0.952. The estimated standard error for the HOF values is 0.1%, which is found based on the repeatability of the pole figure measurements and resulting ODF models presented in Figs. 5 and 6. The difference in HOF values is due to the inherent limitations of the fitting functions, as well as interference from background signals. The Lorentzian function is known for having more pronounced tails and therefore over fits the profile thus leading to low HOF values. The Gaussian distribution also assumes that there are no outliers, and this can lead to some misleading results, in this case very high HOF values

Similar discrepancy in HOF as a result of fitting with Lorentzian and Gaussian functions was reported by Bhattacharyya et al [28]. Practically, we approximate the true HOF of the samples to be between the Gaussian HOF and Lorentzian HOF. With both fits, it can be seen that for acetone-densified sheets, an increase in elongation led to a slight rise in HOF, which is similar to the ODF models discussed. HOF values for ethanol-densified sheets also showed a similar trend, but there was a slight decrease in HOF at 1.5%, which can be attributed to loss of alignment. The full width at half maximum (FWHM) of the distribution is more stable and independent from background values. A reduction in FWHM due to a narrower distribution is indicative of better alignment. FWHM values are also presented in Table 1 and they correspond to the calculated HOF using the fitting functions.

### 3.4. Physical properties of densified sheets

Tensile strength and electrical conductivity data of stretched and densified HA-MWCNT sheets are provided in Fig. 7a and b respectively. Representative stress-strain curves for acetone and ethanol densified sheets are also displayed in Fig. 7c and d. For the acetone-densified sheets, an increase in stretching up to 1% leads to an increase in physical properties such as tensile strength, ultimate strain/elongation, apparent modulus and toughness (indicated by the area under the stress-strain curves in Fig. 7c) as well as improves the electrical conductivity. However, further increase of stretch ratio up to 1.5% led to reduction of all these properties due to breakage and slippage of MWCNT bundles and fibers at elongations close to the failure strain, despite the improvement in alignment.

We notice that for ethanol-densified un-stretched sheets all mechanical and electrical properties are significantly greater/better than un-stretched acetone-densified sheets (30–40% in mechanical properties and almost 50% in electrical conductivity). Moreover, the strong further improvement in properties for ethanol-densified sheets at 0.5% stretching (about 30% across most properties except ultimate strain) significantly contrasts with almost none or slight improvements observed for corresponding acetone-treated sheets. This leads us to believe that longer infiltration time leads to the formation of bigger bundles as discussed before which leads to better load carrying capabilities and charge transfer. At 0.5% elongation, we notice a further improvement in properties for ethanol-densified sheets compared to acetone. For ethanol stretched sheets to 1% elongation, the tensile strength was almost the same as the 0.5% stretched sheets indicating that the main load bearing mechanism established at lower stretch level was due to the tendency of formation of bigger bundles in ethanol. The 0.5%

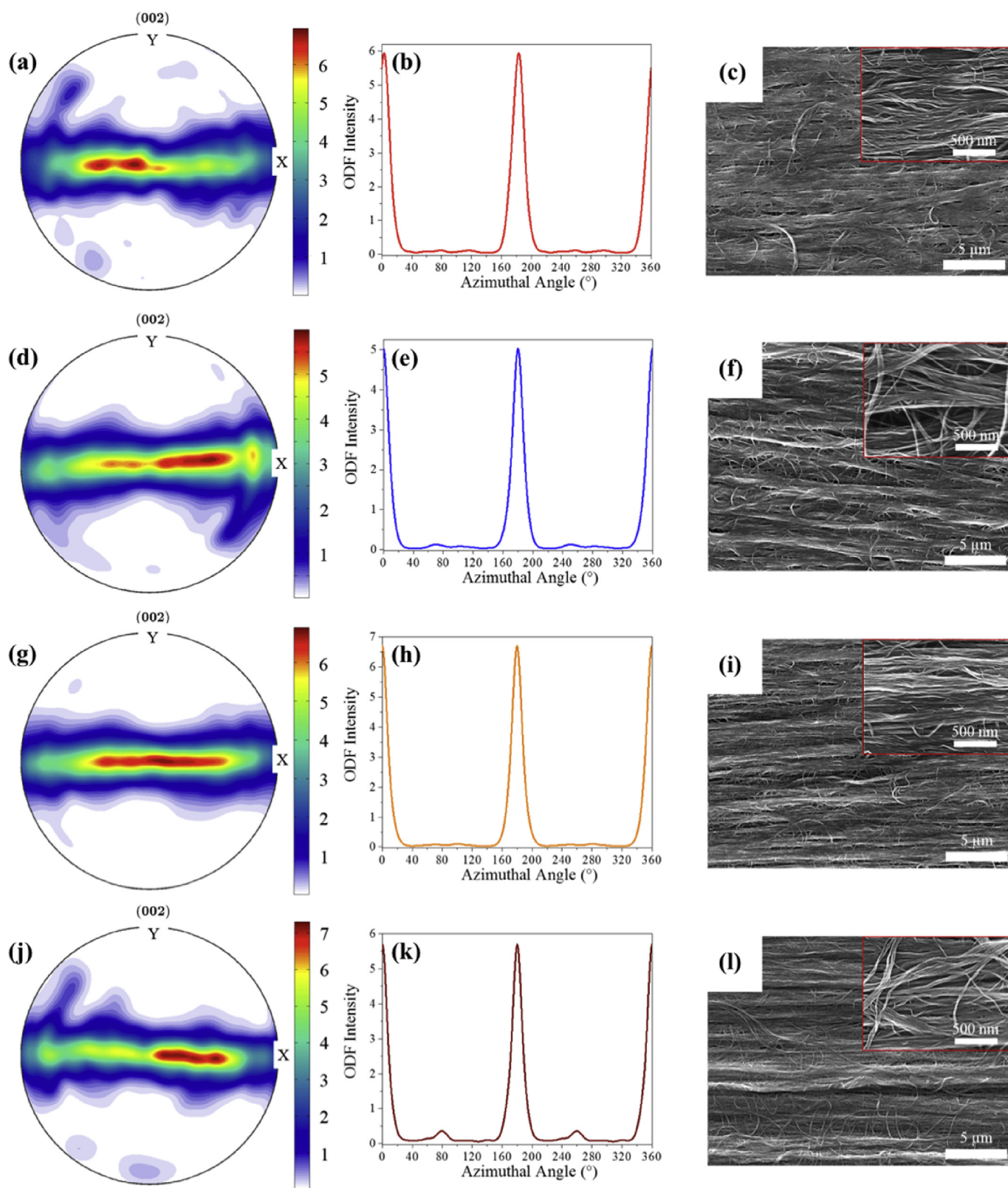


**Fig. 5.** From left to right, ODF model, ODF profile and SEM images (higher magnification in insets) of acetone-densified sheets with (a, b, c) no stretch, (d, e, f) 0.5% stretch, (g, h, i) 1% stretch and (j, k, l) 1.5% stretch. (A colour version of this figure can be viewed online.)

stretched sheets however showed a slight increase in conductivity, which is ascribed to the samples not being fully stretched and aligned at that point and hence tube bundles overlapped each other

(Fig. 6f) offering a better conductive pathway. As expected the 1.5% stretched sheet had a reduction in properties due to breakage and slippage of MWCNTs. Analysis of the stress-strain curves for

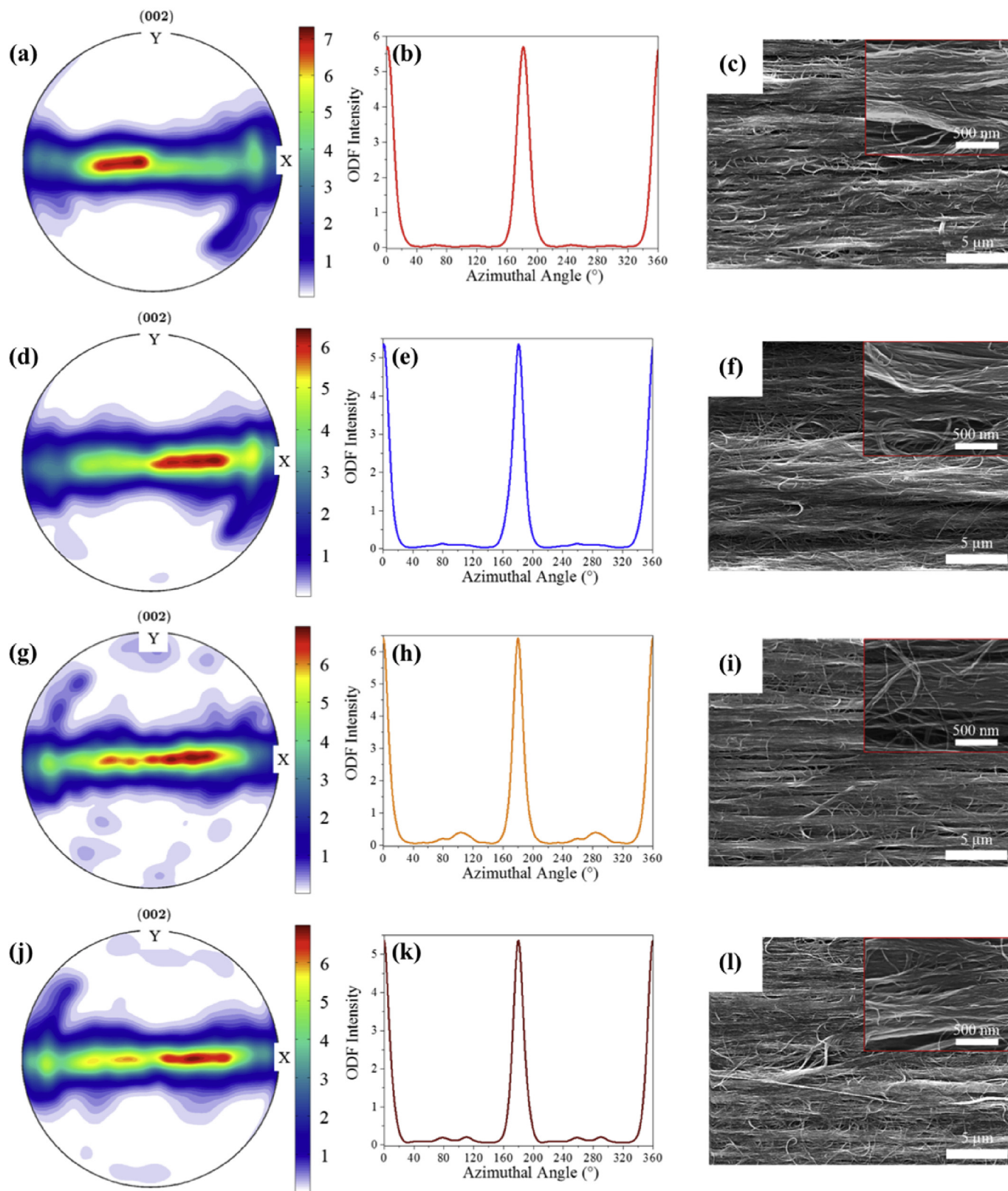


**Fig. 6.** From left to right, ODF model, ODF profile and SEM images (higher magnification in insets) of ethanol-densified sheets with (a, b, c) no stretch, (d, e, f) 0.5% stretch, (g, h, i) 1% stretch and (j, k, l) 1.5% stretch. (A colour version of this figure can be viewed online.)

ethanol-densified sheets show similar modulus (slope of curve) for 0.5% and 1% stretched samples, however 1% stretched sample had the highest toughness (area under the curve). SEM images of

fractured ends for acetone and ethanol-densified sheets are also shown in Fig. 7e and f respectively. The images show an uneven fracture surface with MWCNTs loosely detached at the ends, which

**Table 1**  
HOF values using different fits for acetone and ethanol densified and stretched CNT sheets

Stretch (%)	Acetone densified samples			Ethanol densified samples		
	HOF-L	HOF-G	FWHM ( $^{\circ}$ )	HOF-L	HOF-G	FWHM ( $^{\circ}$ )
0	0.564	0.940	19.20 $\pm$ 0.10	0.557	0.939	19.27 $\pm$ 0.04
0.5	0.570	0.947	17.43 $\pm$ 0.10	0.573	0.948	17.21 $\pm$ 0.16
1	0.572	0.950	16.64 $\pm$ 0.09	0.585	0.957	15.96 $\pm$ 0.15
1.5	0.580	0.953	16.32 $\pm$ 0.15	0.575	0.952	16.99 $\pm$ 0.11

is consistent with sliding of nanotubes/bundles pass each other during deformation [56].

We can conclude that ultimate property improvement by

stretching of solvent densified CNT sheets depends on the solvent properties. Better wettability and lower viscosity of acetone helps to reduce van der Waals forces and therefore, decrease friction between nanotubes, which improves alignment through rearrangement of inter-tube contacts under stretching conditions [4]. In this case, densification resulted in increase of inter-tube contact density due to alignment of tubes at higher level of stretching (elongation). Rise of contact density should result in significant increase of strength and conductivity, but only with the help of stretching. Properties of ethanol (high viscosity, lower wettability and longer infiltration time) support less efficient and slow rearrangement. This resulted in bigger and more aligned bundles with increase of inter-bundle contacts without significant increase of overall inter-tube density (less ultimate tensile strength and

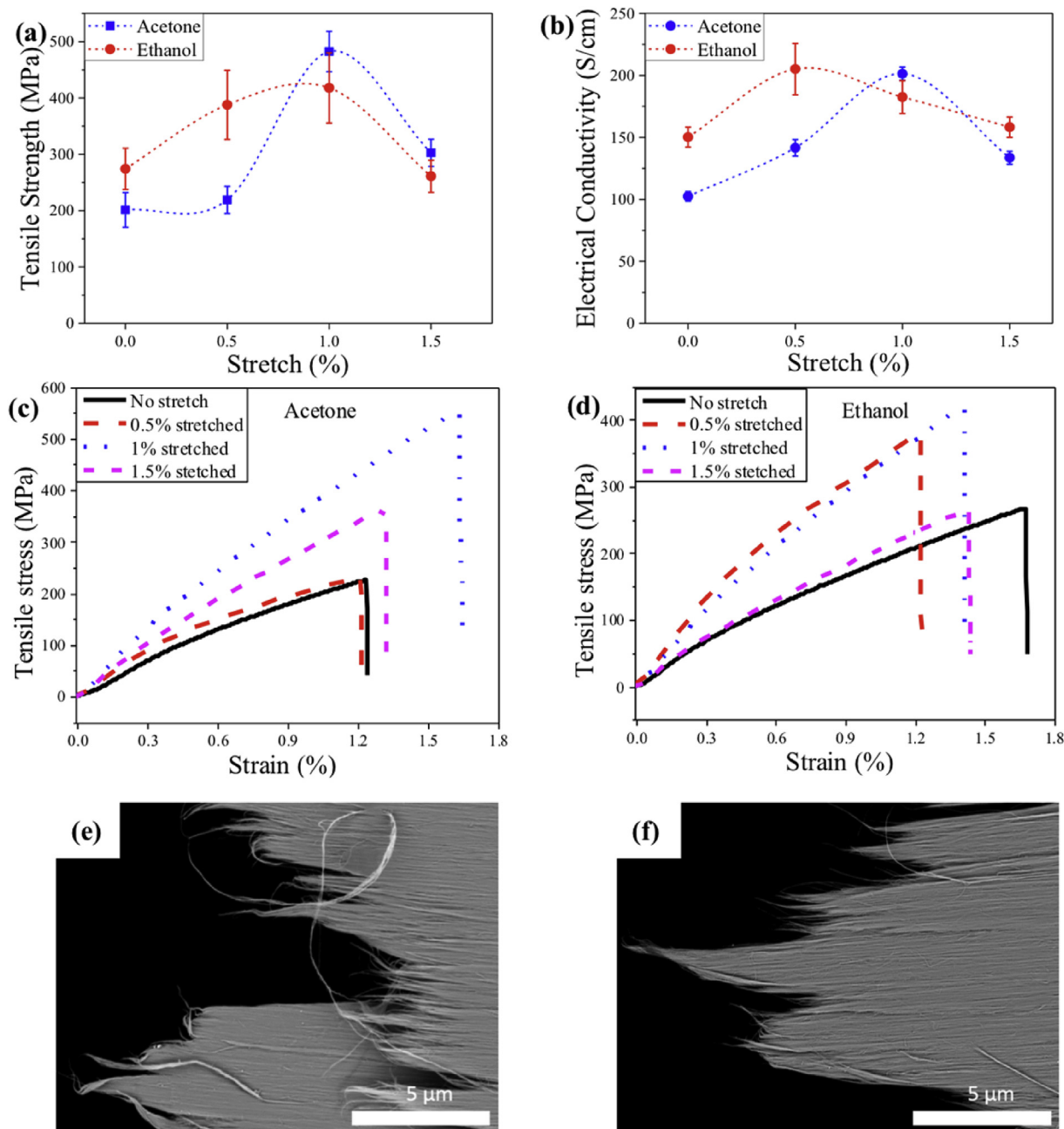


**Fig. 7.** (a) Tensile stress, (b) electrical conductivity and representative stress-strain curves for (c) acetone and (d) ethanol-densified and stretched sheets. SEM images of fractured ends of acetone and ethanol-densified sheets are presented in (e) and (f) respectively. (A colour version of this figure can be viewed online.)

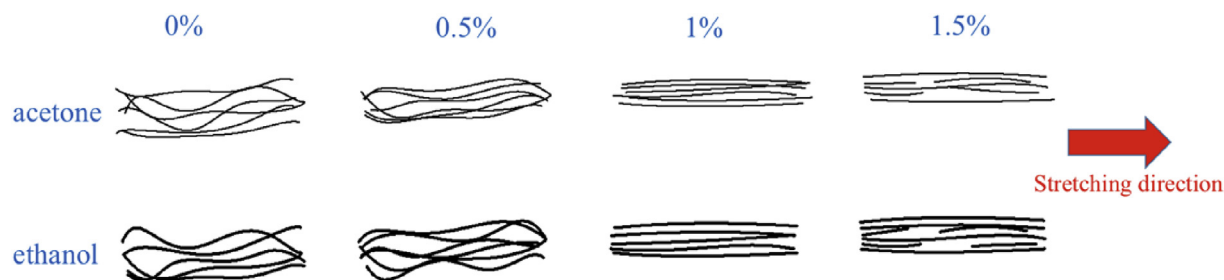


**Fig. 8.** Schematic showing differences in alignment and densification for acetone and ethanol densified sheets. Bolder lines indicate thicker bundles. (A colour version of this figure can be viewed online.)

toughness). All these changes can be achieved and exhausted at low stretching level.

Our data supports the conclusion that the infiltration time and wetting ability of the solvents plays a big role in how the CNT sheets were densified thus affecting their physical properties. A schematic illustrating this difference is shown in Fig. 8. For CNT sheets densified with acetone, which has a faster infiltration time and better wetting ability, we are able to achieve a sheet with dense and uniform properties (indicated by the smaller standard deviation). Ethanol-densified sheets exhibit better properties at non-stretched or low-stretched processing conditions. Stretching in ethanol leads to overall improvement of the mechanical and electrical properties, thus reaching about 30% at 0.5% stretch level. In contrast to ethanol, densification of CNT sheets in acetone at non-stretched and low-stretched conditions does not influence the mechanical and electrical properties a lot. The main improvements in this case were observed at 1% stretching level leading to significant property increase, namely 140% in all mechanical and almost 100% in electrical conductivity. It should be mentioned that the higher standard deviation for ethanol-densified samples can be assigned to the fact that ethanol does not densify the sheets as much as acetone causing uneven properties in the sheets. Similar results, revealing difference between properties of acetone and ethanol-densified sheets, have been reported by Janas et al [57] and Wang et al [4]. The physical properties presented correlate well with the HOF and FWHM results presented in Table 1.

#### 4. Conclusion

This work has demonstrated how pole figure analysis can be used as an accurate method for studying the orientation of different CNT structures. Three different structures were initially analyzed; MWCNT arrays, buckypaper and sheets. The variation in orientation was made evident by the difference in ODF models and profiles and was supported by SEM images. This technique was also applied in studying the difference in alignment of CNT sheets processed by stretching and densification with acetone and ethanol. Acetone and ethanol densified-stretched sheets showed an increase in alignment and physical properties as the elongation was increased. However, other factors came into play when explaining the difference in physical properties for acetone and ethanol densified sheets. For ethanol-densified sheets it was found that the longer infiltration time gave us sheets with bigger bundles, which facilitates good mechanical and electrical properties at 0.5% and 1% elongation. In both cases, an increase in elongation to 1.5% led to a decrease in properties, which was explained by the breakage of bundles during processing. By applying this approach we were able to accurately measure minute changes in alignment of CNT materials processed at different conditions. This technique will be beneficial in evaluating the texture of fibrous CNT assemblages

where such a knowledge is critical in understanding the material's properties.

#### Acknowledgements

This work was funded by the National Science Foundation (NSF) through the following grants: CMMI-0727250; SNM-1120382; ERC-0812348. The authors also appreciate the support of DURIP-ONR N00014-15-1-2473; ARMY W911NF-16-2-0026 and NASA NNX13AF46A grants.

#### Appendix A. Supplementary data

Supplementary data related to this article can be found at <http://dx.doi.org/10.1016/j.carbon.2017.06.028>.

#### References

- [1] A.A. Balandin, Thermal properties of graphene and nanostructured carbon materials, *Nat. Mater.* 10 (8) (2011) 569–581.
- [2] Q.W. Li, Y. Li, X.F. Zhang, S.B. Chikkannavar, Y.H. Zhao, A.M. Dangelewicz, L.X. Zheng, S.K. Doorn, Q.X. Jia, D.E. Peterson, P.N. Arendt, Y.T. Zhu, Structure-dependent electrical properties of carbon nanotube fibers, *Adv. Mater.* 19 (20) (2007) 3358–3363.
- [3] R. Zhang, Q. Wen, W. Qian, D.S. Su, Q. Zhang, F. Wei, Superstrong ultralong carbon nanotubes for mechanical energy storage, *Adv. Mater.* 23 (30) (2011) 3387–3391.
- [4] Y. Wang, M. Li, Y. Gu, X. Zhang, S. Wang, Q. Li, Z. Zhang, Tuning carbon nanotube assembly for flexible, strong and conductive films, *Nanoscale* 7 (7) (2015) 3060–3066.
- [5] S. Li, X. Zhang, J. Zhao, F. Meng, G. Xu, Z. Yong, J. Jia, Z. Zhang, Q. Li, Enhancement of carbon nanotube fibres using different solvents and polymers, *Compos. Sci. Technol.* 72 (12) (2012) 1402–1407.
- [6] X. Sun, T. Chen, Z. Yang, H. Peng, The alignment of carbon nanotubes: an effective route to extend their excellent properties to macroscopic scale, *Acc. Chem. Res.* 46 (2) (2013) 539–549.
- [7] W. Guo, C. Liu, X. Sun, Z. Yang, H.G. Kia, H. Peng, Aligned carbon nanotube/polymer composite fibers with improved mechanical strength and electrical conductivity, *J. Mater. Chem.* 22 (3) (2012) 903–908.
- [8] S. Zhang, K.K. Koziol, I.A. Kinloch, A.H. Windle, Macroscopic fibers of well-aligned carbon nanotubes by wet spinning, *Small* 4 (8) (2008) 1217–1222.
- [9] W. Xu, Y. Chen, H. Zhan, J.N. Wang, High-strength carbon nanotube film from improving alignment and densification, *Nano Lett.* 16 (2) (2016) 946–952.
- [10] K. Jiang, J. Wang, Q. Li, L. Liu, C. Liu, S. Fan, Superaligned carbon nanotube arrays, films, and yarns: a road to applications, *Adv. Mater.* 23 (9) (2011) 1154–1161.
- [11] M. Zhang, S. Fang, A.A. Zakhidov, S.B. Lee, A.E. Aliev, C.D. Williams, K.R. Atkinson, R.H. Baughman, Strong, transparent, multifunctional, carbon nanotube sheets, *Science* 309 (5738) (2005) 1215–1219.
- [12] A.B. Dalton, S. Collins, E. Muñoz, J.M. Razal, V.H. Ebron, J.P. Ferraris, J.N. Coleman, B.G. Kim, R.H. Baughman, Super-tough carbon-nanotube fibres, *Nature* 423 (6941) (2003) 703.
- [13] K. Liu, Y. Sun, L. Chen, C. Feng, X. Feng, K. Jiang, Y. Zhao, S. Fan, Controlled growth of super-aligned carbon nanotube arrays for spinning continuous unidirectional sheets with tunable physical properties, *Nano Lett.* 8 (2) (2008) 700–705.
- [14] J. Di, D. Hu, H. Chen, Z. Yong, M. Chen, Z. Feng, Y. Zhu, Q. Li, Ultrastrong, foldable, and highly conductive carbon nanotube film, *ACS Nano* 6 (6) (2012) 5457–5464.
- [15] C. Jayasinghe, S. Chakrabarti, M.J. Schulz, V. Shanov, Spinning yarn from long carbon nanotube arrays, *J. Mater. Res.* 26 (05) (2011) 645–651.

- [16] Y.-L. Li, I.A. Kinloch, A.H. Windle, Direct spinning of carbon nanotube fibers from chemical vapor deposition synthesis, *Science* 304 (5668) (2004) 276–278.
- [17] W. Li, C. Jayasinghe, V. Shanov, M. Schulz, Spinning carbon nanotube nanofiber under a scanning electron microscope, *Materials* 4 (9) (2011) 1519–1527.
- [18] S. Gbordzoe, R. Malik, N. Alvarez, R. Wolf, V. Shanov, Flexible low-voltage carbon nanotube heaters and their applications, in: Adrián Silva (Ed.), *Advances in Carbon Nanostructures*, InTech, 2016, <http://dx.doi.org/10.5772/64054>. Available from: <https://www.intechopen.com/books/advances-in-carbon-nanostructures/flexible-low-voltage-carbon-nanotube-heaters-and-their-applications>.
- [19] T.H. Nam, K. Goto, H. Nakayama, K. Oshima, V. Premalal, Y. Shimamura, Y. Inoue, K. Naito, S. Kobayashi, Effects of stretching on mechanical properties of aligned multi-walled carbon nanotube/epoxy composites, *Compos. Part A: Appl. Sci. Manuf.* 64 (2014) 194–202.
- [20] S. Li, J.G. Park, Z. Liang, T. Siegrist, T. Liu, M. Zhang, Q. Cheng, B. Wang, C. Zhang, In situ characterization of structural changes and the fraction of aligned carbon nanotube networks produced by stretching, *Carbon* 50 (10) (2012) 3859–3867.
- [21] Q. Cheng, J. Bao, J. Park, Z. Liang, C. Zhang, B. Wang, High mechanical performance composite conductor: multi-walled carbon nanotube sheet/bismaleimide nanocomposites, *Adv. Funct. Mater.* 19 (20) (2009) 3219–3225.
- [22] Q. Liu, M. Li, Y. Gu, Y. Zhang, S. Wang, Q. Li, Z. Zhang, Highly aligned dense carbon nanotube sheets induced by multiple stretching and pressing, *Nanoscale* 6 (8) (2014) 4338–4344.
- [23] T.H. Nam, K. Goto, Y. Yamaguchi, E.V.A. Premalal, Y. Shimamura, Y. Inoue, K. Naito, S. Ogiwara, Effects of CNT diameter on mechanical properties of aligned CNT sheets and composites, *Compos. Part A: Appl. Sci. Manuf.* 76 (2015) 289–298.
- [24] L. Zhang, X. Wang, R. Li, Q. Li, P.D. Bradford, Y. Zhu, Microcombing enables high-performance carbon nanotube composites, *Compos. Sci. Tech.* 123 (2016) 92–98.
- [25] L. Zhang, X. Wang, W. Xu, Y. Zhang, Q. Li, P.D. Bradford, Y. Zhu, Strong and conductive dry carbon nanotube films by microcombing, *Small* 11 (31) (2015) 3830–3836.
- [26] T. Liu, S. Kumar, Quantitative characterization of SWNT orientation by polarized Raman spectroscopy, *Chem. Phys. Lett.* 378 (3–4) (2003) 257–262.
- [27] A.R. Bhattacharyya, T.V. Sreekumar, T. Liu, S. Kumar, L.M. Ericson, R.H. Hauge, R.E. Smalley, Crystallization and orientation studies in polypropylene/single wall carbon nanotube composite, *Polymer* 44 (8) (2003) 2373–2377.
- [28] A.R. Bhattacharyya, T. Sreekumar, T. Liu, S. Kumar, L.M. Ericson, R.H. Hauge, R.E. Smalley, Crystallization and orientation studies in polypropylene/single wall carbon nanotube composite, *Polymer* 44 (8) (2003) 2373–2377.
- [29] J. Hwang, H. Gommans, A. Ugawa, H. Tashiro, R. Haggenmueller, K.I. Winey, J.E. Fischer, D. Tanner, A. Rinzler, Polarized spectroscopy of aligned single-wall carbon nanotubes, *Phys. Rev. B* 62 (20) (2000) R13310.
- [30] H. Gommans, J. Alldredge, H. Tashiro, J. Park, J. Magnuson, A. Rinzler, Fibers of aligned single-walled carbon nanotubes: polarized Raman spectroscopy, *J. Appl. Phys.* 88 (5) (2000) 2509–2514.
- [31] X. Wang, Z.Z. Yong, Q.W. Li, P.D. Bradford, W. Liu, D.S. Tucker, W. Cai, H. Wang, F.G. Yuan, Y.T. Zhu, Ultrastrong, stiff and multifunctional carbon nanotube composites, *Mater. Res. Lett.* 1 (1) (2012) 19–25.
- [32] B.N. Wang, R.D. Bennett, E. Verploegen, A.J. Hart, R.E. Cohen, Quantitative characterization of the morphology of multiwall carbon nanotube films by small-angle X-ray scattering, *J. Phys. Chem. C* 111 (16) (2007) 5859–5865.
- [33] M. Bedewy, E.R. Meshot, H. Guo, E.A. Verploegen, W. Lu, A.J. Hart, Collective mechanism for the evolution and self-termination of vertically aligned carbon nanotube growth, *J. Phys. Chem. C* 113 (48) (2009) 20576–20582.
- [34] E.R. Meshot, M. Bedewy, K.M. Lyons, A.R. Woll, K.A. Juggernaut, S. Tawfik, A.J. Hart, Measuring the lengthening kinetics of aligned nanostructures by spatiotemporal correlation of height and orientation, *Nanoscale* 2 (6) (2010) 896–900.
- [35] P. Mahanandia, J.J. Schneider, M. Engel, B. Stühn, S.V. Subramanyam, K.K. Nanda, Studies towards synthesis, evolution and alignment characteristics of dense, millimeter long multiwalled carbon nanotube arrays, *Beilstein J. Nanotechnol.* 2 (2011) 293–301.
- [36] E. Moaseri, M. Karimi, M. Baniadam, M. Maghrebi, Improvements in mechanical properties of multi-walled carbon nanotube-reinforced epoxy composites through novel magnetic-assisted method for alignment of carbon nanotubes, *Compos. Part A: Appl. Sci. Manuf.* 64 (2014) 228–233.
- [37] G. Yi, L. Zhuo, L. Ziyin, Z. Liangjia, T. Allen, B. Sylvain, C.P. Wong, Automated dispersion and orientation analysis for carbon nanotube reinforced polymer composites, *Nanotechnology* 23 (43) (2012) 435706.
- [38] J. Hwang, H.H. Gommans, A. Ugawa, H. Tashiro, R. Haggenmueller, K.I. Winey, J.E. Fischer, D.B. Tanner, A.G. Rinzler, Polarized spectroscopy of aligned single-wall carbon nanotubes, *Phys. Rev. B* 62 (20) (2000) R13310–R13313.
- [39] U. Vainio, T.I.W. Schnoor, S. Koyiloth Vayalil, K. Schulte, M. Müller, E.T. Lilleodden, Orientation distribution of vertically aligned multiwalled carbon nanotubes, *J. Phys. Chem. C* 118 (18) (2014) 9507–9513.
- [40] X. Yang, L. Yuan, V.K. Peterson, A.I. Minett, M. Zhao, N. Kirby, S. Mudie, A.T. Harris, Pretreatment control of carbon nanotube array growth for gas separation: alignment and growth studied using microscopy and small-angle X-ray scattering, *ACS Appl. Mater. Interfaces* 5 (8) (2013) 3063–3070.
- [41] S. Boncel, J. Górka, M.S.P. Shaffer, K.K.K. Koziol, Shear-induced crystallisation of molten isotactic polypropylene within the intertube channels of aligned multi-wall carbon nanotube arrays towards structurally controlled composites, *Mater. Lett.* 116 (2014) 53–56.
- [42] J.J. Vilatela, D.L. I.A. Kinloch, R.J. Young, A.H. Windle, Structure of and stress transfer in fibres spun from carbon nanotubes produced by chemical vapour deposition, *Carbon* 49 (2011) 4149–4158.
- [43] U. Vainio, T.I.W. Schnoor, S.K. Vayalil, K. Schulte, M. Müller, E.T. Lilleodden, Orientation distribution of vertically aligned multiwalled carbon nanotubes, *J. Phys. Chem. C* 118 (18) (2014) 9507–9513.
- [44] S. Suwas, N.P. Gurao, Crystallographic texture in materials, *J. Indian Inst. Sci.* 88 (2) (2012) 151–177.
- [45] C. Burger, B.S. Hsiao, B. Chu, Preferred orientation in polymer fiber scattering, *J. Macromol. Sci. Polym. Rev.* 50 (1) (2010) 91–111.
- [46] B. Schrauwen, L.v. Breemen, A. Spoelstra, L. Govaert, G. Peters, H. Meijer, Structure, deformation, and failure of flow-oriented semicrystalline polymers, *Macromolecules* 37 (23) (2004) 8618–8633.
- [47] J. Jia, D. Raabe, Crystallinity and Crystallographic Texture in Isotactic Polypropylene during Deformation and Heating, 2008 arXiv preprint arXiv:0811.2412.
- [48] J. Butler, S. Wap, F. Chambon, Quantitative pole figure analysis of oriented polyethylene films, *Adv. X-ray Anal.* 2000 (43) (2000) 141–150.
- [49] N.T. Alvarez, P. Miller, M. Haase, N. Kienzle, L. Zhang, M.J. Schulz, V. Shanov, Carbon nanotube assembly at near-industrial natural-fiber spinning rates, *Carbon* 86 (2015) 350–357.
- [50] D.N. Futaba, T. Yamada, K. Kobashi, M. Yumura, K. Hata, Macroscopic wall number analysis of single-walled, double-walled, and few-walled carbon nanotubes by X-ray diffraction, *J. Am. Chem. Soc.* 133 (15) (2011) 5716–5719.
- [51] Y. Yun, V. Shanov, Y. Tu, S. Subramaniam, M.J. Schulz, Growth mechanism of long aligned multiwall carbon nanotube arrays by water-assisted chemical vapor deposition, *J. Phys. Chem. B* 110 (47) (2006) 23920–23925.
- [52] X. Zhang, X. Yu, J. Zhao, Q. Li, Bio-inspired design and fabrication of super-strong and multifunctional carbon nanotube composites, in: *Carbon Nanotubes - Current Progress of their Polymer Composites*, 2016.
- [53] E. Dujardin, T. Ebbesen, H. Hiura, K. Tanigaki, Capillarity and wetting of carbon nanotubes, *Science* 265 (5180) (1994) 1850–1852.
- [54] S. Boncel, K.Z. Walczak, K.K. Koziol, Dynamics of capillary infiltration of liquids into a highly aligned multi-walled carbon nanotube film, *Beilstein J. Nanotechnol.* 2 (1) (2011) 311–317.
- [55] J.J. Vilatela, L. Deng, I.A. Kinloch, R.J. Young, A.H. Windle, Structure of and stress transfer in fibres spun from carbon nanotubes produced by chemical vapour deposition, *Carbon* 49 (13) (2011) 4149–4158.
- [56] R. Malik, C. McConnell, N.T. Alvarez, M. Haase, S. Gbordzoe, V. Shanov, Rapid, in situ plasma functionalization of carbon nanotubes for improved CNT/epoxy composites, *RSC Adv.* 6 (110) (2016) 108840–108850.
- [57] D. Janas, K.K. Koziol, Improved performance of ultra-fast carbon nanotube film heaters, *J. Autom. Control Eng.* 2 (2) (2014).